Available online at www.sciencedirect.com

ScienceDirect

Procedia Engineering 130 (2015) 1288 – 1297

Procedia Engineering

www.elsevier.com/locate/procedia

14th International Conference on Pressure Vessel Technology

3-D Interaction of a Corner Flaw with a Non-Aligned Surface Flaw in an Infinitely Large Plate under Tension

Q. Ma[a,*], C. Levy[b], M. Perl[c]

[a]*Edward F. Cross School of Engineering, Walla Walla University, College Place, WA 99324, USA*
[b]*Dept. of Mechanical and Materials Engineering, Florida International University, Miami, FL 33199 USA*
[c]*Pearlstone Center for Aeronautical Engineering Studies, Dept. of Mechanical Engineering, Ben Gurion University of the Negev, Beer Sheva 84105 ISRAEL*

Abstract

The evaluation of non-aligned multiple flaws is required in various Fitness-for-Service codes. For non-aligned parallel cracks, on-site inspection needs to decide whether they should be treated as coalesced or separate multiple cracks for Fitness-for-Service. Criteria and standards for the adjustment of multiple nonaligned cracks are very different from one source to another in the existing literature. And those criteria and standards are often derived from on-site service experience without rigorous and systematic verification. Based on this observation, the authors previously reported on the interaction between an edge and an embedded parallel crack in 2-D scenarios. Since crack configurations detected using non-destructive methods in the real world are generally 3-D in nature, the study of 3-D interaction of non-aligned flaws is deemed necessary in order to obtain more practical guidance in the usage of rules speculated in Fitness-for-Service. In this study, the 3D interaction between a corner flaw and a non-aligned parallel surface flaw in an infinitely large plate is investigated to correlate better the criteria and standards from various resources in recommending the usage of those standards for the purpose of Fitness-for-Service and to classify them as either conservative or non-conservative.

Peer-review under responsibility of the organizing committee of ICPVT-14

Keywords: Stress Intensity Factors; Crack; Non-aligned; Flaws; Fitness-for-Service;

* Corresponding author. Tel.: (509)527-2537; fax: (509)527-2867.
E-mail address: qin.ma@wallawalla.edu

Peer-review under responsibility of the organizing committee of ICPVT-14
doi:10.1016/j.proeng.2015.12.299

1. Introduction

The interaction of multiple flaws plays an important role in the cracking behavior due to degradation of plant components, especially in the case of stress corrosion cracking (SCC) and fatigue [1, 2]. The Fitness-for-Service standards require the characterization of multiple flaws to evaluate structural integrity of the flawed components using fracture mechanics concepts. The first step is to determine if the multiple flaws lie on the same cross-sectional plane to be considered aligned flaws, or whether they lie on parallel planes and considered to be non-aligned parallel flaws using flaw alignment rules. There are several flaw alignment rules that can be considered for in-service evaluations, such as those found in the American Society of Mechanical Engineers Boiler and Pressure Vessel Code Section XI (ASME Section XI) [3], Guide to Methods for Assessing the Acceptability of Flaws in Metallic Structures [4], European Fitness-for-Service Network (FITNET) [5], American Petroleum Institute (API) 571-1/ASME FFS-1 [6], or Rules on Fitness-for-Service for Nuclear Power Plant Components in the Japan Society of Mechanical Engineers (JSME, S NA1-2008) [7]. These rules differ from each other and some alignment rules may provide overly conservative results while others give non-conservative assessments

Nomenclature

a_1	half embedded internal flaw length
a_2	edge flaw length
H	vertical flaw separation dimension
S	horizontal flaw separation dimension
u,v,w	nodal displacements
r	radial distance
E	Young's modulus
G	Shear modulus
K_I	mode I SIF
K_{IS}	mode I SIF due to at the edge flaw tip S
K_0	Normalizing SIF
P	applied tensile load
GREEK SYMBOLS	
υ	Poisson's ratio
σ_y	yield stress
ϕ	parametric angle

In recent years there have been some intensive studies regarding the interaction of multiple non-aligned flaws in cases of two offset parallel embedded flaws contained in a large steel plate. For example, Kamaya [8] studied the growth evaluation of multiple interacting surface cracks by combination of numerical methods and experimental studies. Hasegawa et al. [9] studied the interaction of two parallel embedded non-aligned flaws for Fitness-for-Service based on LEFM. In their most recent studies Hasegawa et al. [10-12], Miyazaki et al. [12], and Suga et al. [13-14] considered plastic collapse behavior for dissimilar non-aligned flaws.

However, none of the aforementioned investigations addressed the interaction of multiple flaws where one of the flaws is an edge flaw. A recent study by Ma et al. [15] addressed the issue of an embedded flaw interacting with an edge flaw based on 2-D analysis. Interaction of an embedded flaw with an edge flaw with a 3-D crack configuration has not been addressed in literature, so far. Based on this observation, the objective of this study is to investigate the influence of an embedded flaw or an embedded semi-circular surface crack, on the fracture behavior of an edge flaw, or a quarter-circle edge corner crack, in an infinitely large solid. Specifically, the stress intensity factors (SIFs) along the crack front of the edge flaw have been studied for a wide range of the normalized gap, H/a_2 = 0.4~2, and the normalized separation distance, S/a_2 = -0.4~2 (see Fig. 1), between cracks on parallel planes based on the principle of linear elastic fracture mechanics (LEFM). The designations used here are the same as those in the recent study by

Ma et al. [15]. In order to simplify the analysis and make the results comparable with the previous 2-D results, only a circular crack configuration is considered in this study. In other words, the 2-D crack size, denoted as a_1, becomes the radius of the 3-D semi-circular embedded crack. And the edge crack size, denoted as a_2, becomes the radius of the 3-D quarter-circle crack at the edge corner. The analysis results show that the 3-D SIFs exhibit a distinct interaction behavior with the 2-D analysis results. At the same time, the 3D SIFs are in general found much lower in magnitude than their 2-D counterparts. The conclusions drawn however are similar to those of the 2-D analysis. That is, certain existing standards/criteria provide results that are much more conservative than others while certain ones do not provide adequate information for application.

2. Solid Modeling

Figure 1 depicts an infinitely long plate or solid containing a quarter-circle edge corner crack of radius a_2, and an embedded semi-circular surface crack of radius a_1, used for this study. The plate is assumed to be made of steel with Young's modulus E=200 GPa, Poisson's ratio $\upsilon=0.3$, and yield stress σ_y=304 MPa. The remote tensile load is taken as p = 2 kPa. The remote tensile load is applied onto the top surface of the plate while the bottom surface of the plate is fixed.

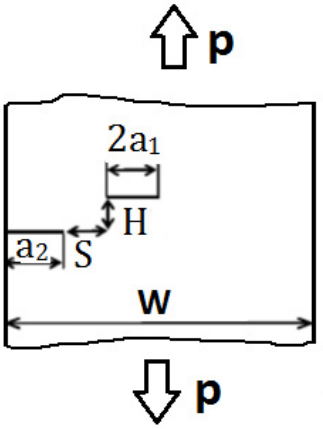

Fig. 1. An infinitely long plate having two non-aligned flaws, namely, an edge crack interacting with an embedded crack. Identical parametric notations are used as in [15].

For all cases, the plate is considered elastic and infinitely long in size. The width of the plate is W and its depth D (not shown on the graph). The flaws planes are always assumed to be perpendicular to the load applied. The flaw separation distance is S parallel to the flaw surfaces and the gap between the flaws is H perpendicular to the flaw surfaces. The plate is assumed "infinite" in all dimensions relative to the cracks' size.

3. Finite Element Idealization

The model is solved using the standard FE code ANSYS [16]. A global mesh of the entire plate, shown in Fig. 2(a), is generated using 10-node tetrahedron elements (SOLID92). The 10-node tetrahedron element has a quadratic displacement behavior and is well suited to model irregular meshes, specifically for a plate with an edge and an internally embedded flaws. The elements are varied in size, small near the flaw region and gradually increased when moving away from it as shown in Fig. 2(b). In the crack vicinity, a small volume was created to encompass the two interacting cracks. By creating this small volume, it becomes much easier to control the mesh quality along the crack fronts and the vicinity of the cracks. At the same time, it also helps to reduce the total DOFs needed and thus

increase the accuracy of results.

The SIFs are solved using the submodeling technique adopted in the previous work by Ma [17], and Levy et. al [18]. Figures 2(c) depicts a toroid-like submodel of a full crack model with a quarter-circle crack configuration. Generally speaking, the submodel is constructed by 20-node isoparametric solid brick elements (SOLID95) and made of three layers containing the two crack surfaces, which are created with a small opening from the deepest line of the crack surface [17]. The first layer of elements consists of 160 20-node isoparametric elements that are collapsed to form the wedges to accommodate the singularity at the crack front. On top of this layer, are two additional layers consisting of 20-node, isoparametric elements. The sub-model consists of a total of 6543 degrees of freedom enabling the accurate evaluation of the SIF distribution along the crack front at intervals of 9 deg. from for ϕ=0 to 90 deg. The radial length of the sub-model is $2*a_2/3$ for the quarter-circle crack.

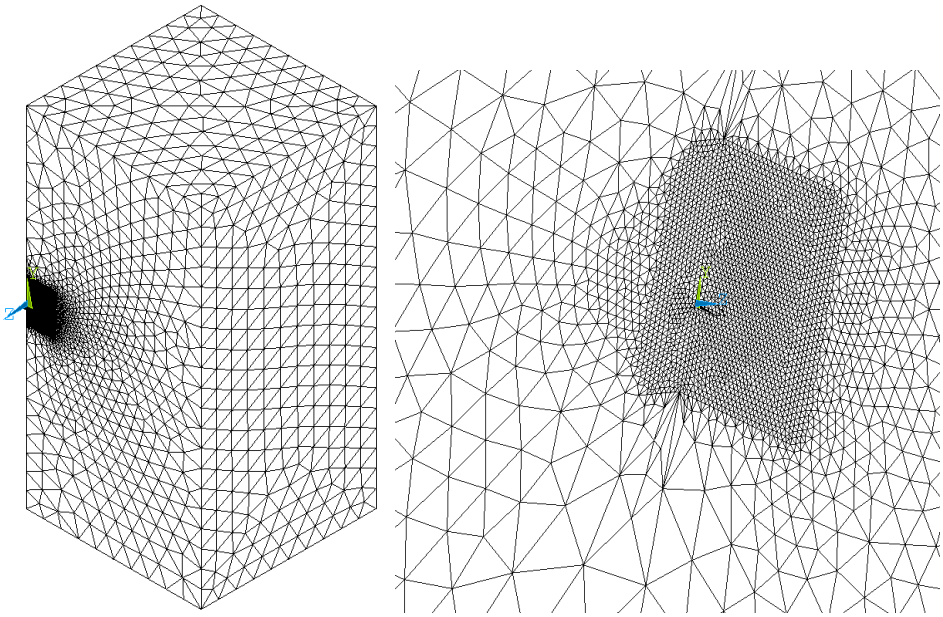

(a) A typical global mesh (b) A typical mesh in the vicinity of the flaws

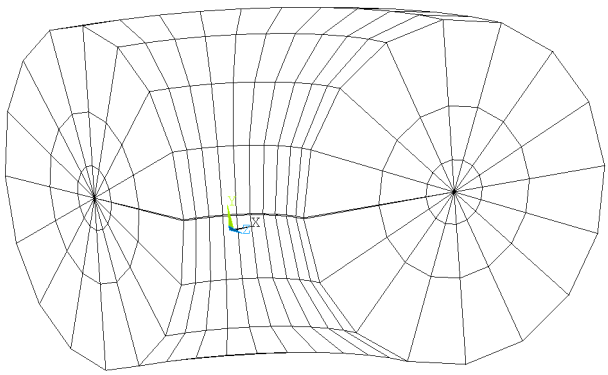

(c) The toroid-like submodeling

Fig. 2. The Finite Element Model; (a) A typical global mesh; (b) A typical mesh in the vicinity of the flaws; (c) The submodel showing the toroid-like finite element mesh.

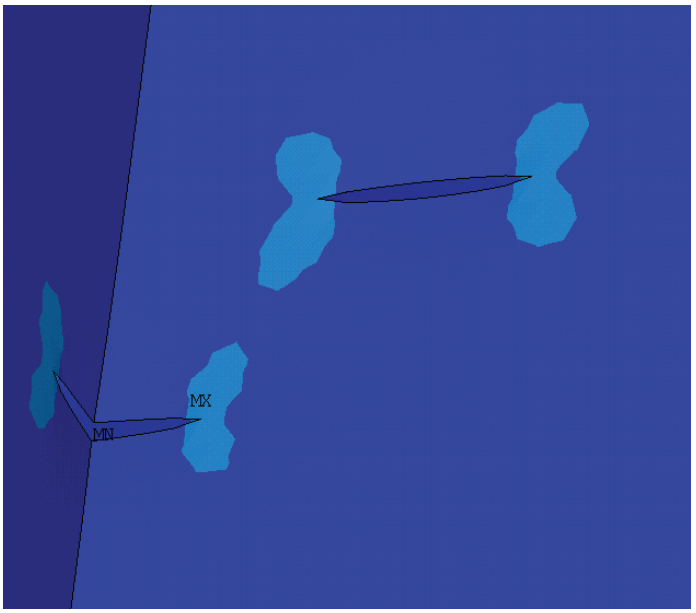

Fig. 3. A typical contour plot of von Mises stress in the vicinity of the flaws.

Convergence tests were performed using the stress intensity factor as the convergence criterion. In brief, based on the trial and error methodology, it is anticipated, for most cases, that the level of error was approximately less than 5% for meshes having more than 200,000 DOFs, about half of them being assigned to the small volume. Typical meshes for the coarse model included about 50,000 elements with approximately 60,000 nodes. The option where the software automatically adjusted element shapes and aspect ratios for all meshes was always chosen. A typical stress contour is given in Fig. 3 to demonstrate the interaction behavior between the two 3-D flaws.

4. Results and Discussions

The interaction behavior of a corner crack with an embedded surface crack depends on multiple factors including the normalized horizontal separation distance between the two cracks S/a_2, the normalized vertical separation distance H/a_2, and the relative crack size a_1/a_2. Since only circular-type crack configurations are the focus of this study, crack shape effect will be discussed elsewhere

4.1. The Effects of Flaw Spacing for Similar Flaw Sizes

In order to make the investigation less complicated, our first focus is on cases with similar flaw sizes i.e., $a_1=a_2$. As an extreme, when the size of the edge crack is the same as the size of the embedded crack, the interaction behavior is solely influenced by relative separation alone.

Figure 4 depicts the normalized SIF distribution along the crack front for a quarter-circle corner crack, a_2=15mm, interacting with an embedded semi-circular crack, a_2=15mm, in an infinitely large plate under tension. The vertical separation distance is constant $H/a_2 = 0.4$ and the relative flaw size is $a_1/ a_2= 1$. The SEC curve represents the numerical solution for a single edge crack (SEC). Clearly, this SEC curve provides a bound for the SIFs when an edge crack interacts with an embedded one.

The results presented are for the case of a fixed vertical separation distance between the two cracks such that $H/a_2 = 0.4$, which is the smallest vertical separation distance studied for the case of two parallel cracks that are identical in crack size. The normalized horizontal separation distance is $S/a_2 = -0.4\sim2$. For any given value of the horizontal separation distance S/a_2, SIFs increase along the crack front as ϕ increases with a maximum normalized SIF at

ϕ=90°. For any point along the crack front, the smaller the normalized separation space S/a_2, the larger the SIF magnitude. Note here that negative S/a_2 means the parallel flaws overlap. It is clear that the SEC curve provides the lower bound for this case.

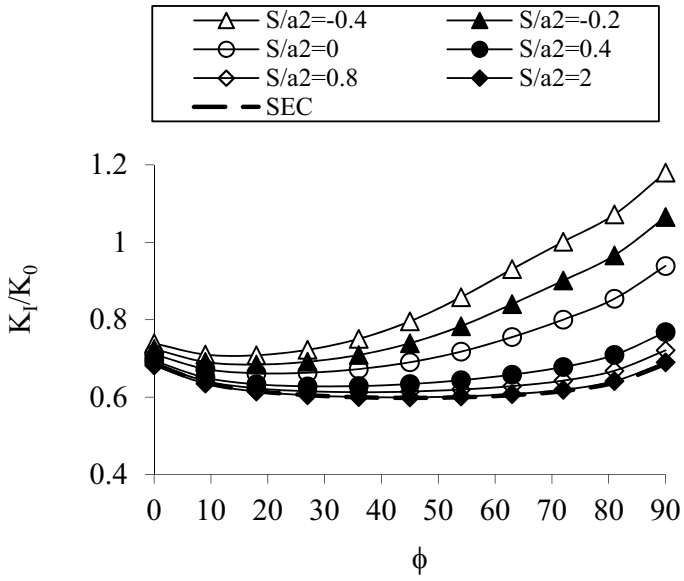

Fig. 4. The normalized SIF distribution along the crack front for a quarter-circle edge corner crack interacting with an embedded semi-circular crack in an infinitely large solid under tension for $H/a_2 = 0.4$ (a_2 = 15mm; $2a_1$=30mm). Negative S/a_2 represents overlapping parallel flaws.

The interaction behavior of the maximum SIFs is of great interest in this study. Figure 5 shows the maximum normalized SIFs versus the normalized horizontal separation space S/a_2 as a function of H/a_2 for a quarter-circle edge corner crack interacting with an embedded semi-circular crack in an infinitely large solid. The relative crack size of the two interacting cracks is a_1/a_2=1.

We see that the normalized maximum SIFs, K_{Imax}/K_0, decrease as the embedded flaw moves away from the surface flaw, i.e., when H/a_2 increases. For example, for the case of H/a_2=0.4, the normalized maximum SIFs decrease with the increase of the horizontal separation space S/a_2 significantly and monotonically from the overlapping range starting at S/a_2 =-0.4. This decreasing trend of the maximum SIFs continues until it reaches approximately the value of the maximum SEC SIF value at $S/a_2 \geq 1$. That is to say, as the embedded flaw moves away from the edge flaw by a larger distance of $S/a_2 > 1$, the edge flaw will no longer "feel" the influence of the presence of the embedded flaw. In this case, the embedded flaw can be treated as a separate flaw in the fitness-for-service considerations. This observation is identical to what is seen from the 2-D analysis [15].

However, there is a significant difference between the 2-D and 3-D crack interaction behaviors when considering the overall trend of the maximum 3-D SIFs varying with the separation space S/a_2 and comparing it with the 2-D analysis by Hasegawa et al. [9] and Ma et al. [15]. In case of 2-D, for each case of a fixed value of H/a_2, the normalized SIF, K_{IS}/K_0 starts to decrease after it reaches its peak value at certain normalized horizontal distance S/a_2. And the peak value is not necessarily always at $S/a_2 = 0$. This type of 2-D interaction behavior is not observed from the present 3-D analysis. In other words, the interaction behavior from the 3-D analysis shows almost exclusively a decreasing trend with the increase of the horizontal separation space S/a_2.

In the meantime, we also observe (Fig. 5) the significant influence of the relative separation distance in the vertical direction H/a_2 on the maximum SIFs. With the increase of the relative vertical separation distance, H/a_2, for the case of a_2 = 15mm and $2a_1$=30mm, when $H/a_2 \geq 0.8$, the maximum SIFs approach to the maximum SEC SIF

value. That is to say, the maximum SIFs become insensitive to the variation of the relative horizontal separation space S/a2 once the H/a_2 is sufficiently large. If this occurs, there would be no interaction between the embedded flaw and the crack in the fitness-for-service considerations.

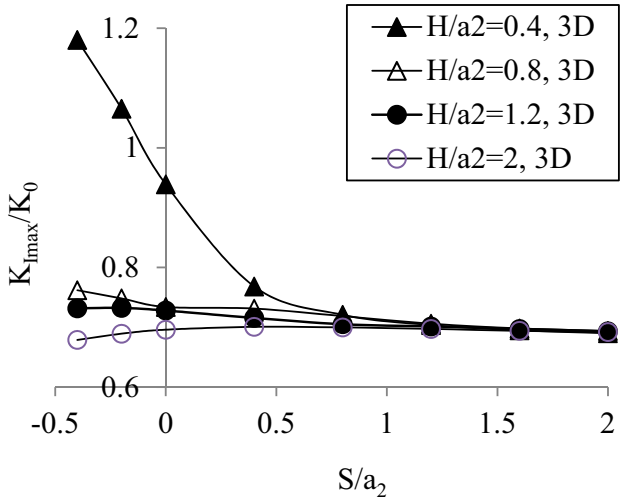

Fig. 5. The maximum normalized SIFs vs. S/a_2 as a function of H/a_2 for a quarter-circle edge corner crack interacting with an embedded semi-circular crack in an infinitely large solid under tension (a_2 = 15mm; $2a_1$=30mm).

The tendency of interaction between an edge corner quarter-circle crack and an embedded semi-circular surface crack can be demonstrated for cases with similar flaw size combinations. However, the significance of interaction due to various combinations of flaw size and separation parameters does vary tremendously, which indicates the interaction of flaws is influenced by the multiple parameters mentioned previously. And the alignment rules should reflect this aspect in order to capture the multifaceted parametric effects.

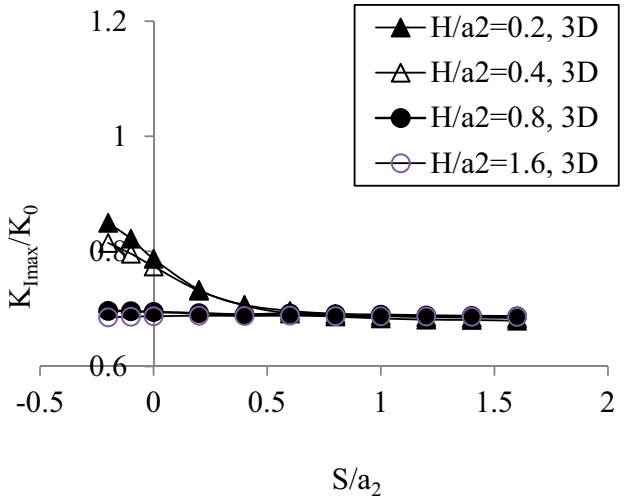

Fig. 6. The maximum normalized SIFs vs. S/a_2 as a function of H/a_2 for a quarter-circle edge corner crack interacting with an embedded semi-circular crack in an infinitely large solid under tension (a_2 = 10mm; $2a_1$=10mm).

Figure 6 demonstrates the interaction of the embedded semi-circular surface crack towards the quarter-circle edge corner crack when the length of the edge crack is taken as a_2=10 mm but the embedded crack size is taken as a_1 = 5 mm. This case is much smaller than the previous case shown in Fig. 5. In this case, the relative crack size is a_1/a_2= 1/2. Considering a similar range of vertical separation for H/a_2 = 0.4-1.6, we see that the magnitude of the max value of the normalized SIFs has dropped from ~1.2 to ~0.82 for the case of H/a_2 =0.4 at S/a_2=-0.4 in Fig. 10 and H/a_2 =0.4 at S/a_2=-0.2 in Fig. 6. At the same time, we see a much smaller interaction range when comparing results in Fig. 5 to those in Fig. 6. For example, H/a2=0.4 case has an interaction range between -0.5 and 1.2 in Fig. 5, whereas it is from -0.2 to 0.6 in Fig. 6. That is to say, if the vertical separation distance is kept the same and the relative size of the embedded flaw a_1/a_2 becomes smaller, its influence on the maximum SIFs along the edge crack front dies out quicker.

4.2. The Effects of Flaw Spacing for Short Embedded Flaws

Figure 7 demonstrates the interaction behavior of the two cracks when the embedded semi-circular crack is significantly smaller than the quarter-circle edge corner crack. In this case, the relative crack size is a_1/a_2= 1/3. Again considering a similar range of vertical separation for H/a_2 =0.2-1.2, we see that the magnitude of the max value of the normalized SIFs has dropped from ~1.2 for the case of H/a_2 =0.4 at S/a_2=-0.4 in Fig. 5 to ~0.74 for the case of H/a_2 =0.4 at S/a_2=-0.2 in Fig. 7. At the same time, we see a much smaller interaction range is presented in Fig. 7 for S/a_2 = -0.2 to 0.4 instead of S/a_2 = -0.4 to 1 in Fig. 5 for the same value of H/a_2=0.4. The results presented in Fig. 7 are apparently similar to those in Fig. 6. This indicates the influence of the relative crack size of a_1/a_2 on the interaction behavior of the two parallel cracks is significant. We also note that the differences in K_{Imax}/K_0 values between the different values of H/a_2 become much smaller when a_1/a_2 become smaller for constant S/a_2.

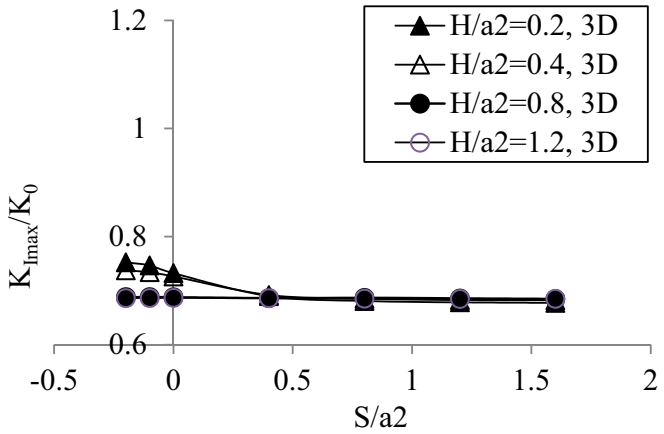

Fig. 7. The maximum normalized SIFs vs. S/a_2 as a function of H/a_2 for a quarter-circle corner crack interacting with an embedded semi-circular crack in an infinitely large solid under tension (a_2 = 15mm; $2a_1$=10mm).

4.3. The Influence of Flaw Alignment Rules

Figure 8 shows the same 3-D results of Fig. 5, but with the criteria included from two different Fitness-in-Service sources [4, 5]. The thick dashed curve illustrates the effect of the British Standards flaw alignment rules (BritS) [4] while the dotted-dashed curve illustrates the effect of the flaw alignment rules imposed by FITNET [5].

Due to the BritS, the criterion is given as

$$S_1 \leq a_1 + a_2 \tag{1}$$

where S_1 is the distance connecting the crack tip of the edge flaw and the tip of the embedded crack closest to the flaw.

By the FITNET, the criterion is given as

$$H \le \min\left(2a_1, a_2\right) \tag{2}$$

The BritS apparently considers the effect of separation parameters of both relative vertical distance, H/a_2, and the relative horizontal distance, S/a_2, as well as the relative flaw size, a_1/a_2, in an implicit manner. The dashed curve was obtained considering the following relationship from the criterion by (1):

$$\frac{H}{a_2} \le \sqrt{\left(\frac{a_1}{a_2}+1\right)^2 - \left(\frac{S}{a_2}\right)^2} \tag{3}$$

Therefore, based on the BritS, each point on the thick dashed curve corresponds to a different value of vertical separation distance H/a_2. The criterion reflects the influence of all the relative parameters of S/a_2, H/a_2 and a_1/a_2.

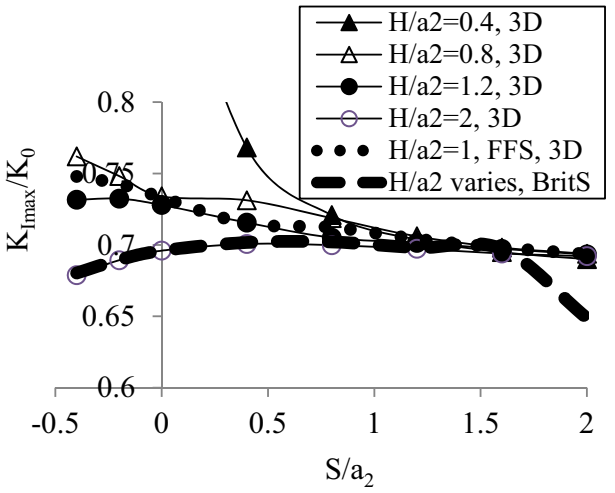

Fig. 8. Normalized SIFs vs. S/a_2 as a function of H/a_2 for edge-embedded flaws (a_2 = 15mm; $2a_1$=30mm) with FITNET standard and BritS standard.

But the FITNET does not include any effect from the horizontal separation dimension, S/a_2, which is an important parameter that influences the SIF values. In fact, for the case presented in Fig. 8, the min ($2a_1$, a_2) is a_2=15mm, and thus H/a_2 = 1. Thus the thick dotted-dashed curve was obtained under a constant relative separation distance H/a_2 in the same manner as that for other cases under constant H/a_2 values.

The two criteria apparently provide very different scenarios for the judgment of alignment vs. non-alignment for two parallel offset flaws, which is the same as observed from the recent 2-D analysis results [15]. For certain flaw separation conditions, one criteria may consider the same two flaws on parallel planes to act as one while the other criteria will suggest that the flaws should be considered as separate ones. The critical values from the BritS and the FITNET rules as demonstrated in Fig. 8 clearly show that the FITNET will provide a much higher barrier for the flaws to be judged as aligned ones. Thus the FITNET is a much more conservative rule. At the same time, the BritS provides much lower critical values of the SIFs. It thus provides non-conservative results in fitness-for-service applications. The results from other standards [3, 6, 7], though not presented in this paper, are perceived to bear the same behavior in the same manner as discussed here.

5. Concluding Remarks

In this study, the interaction behavior of two parallel cracks in an infinitely large plate has been investigated. The SIF along the crack front of a quarter-circle edge corner crack affected by an embedded semi-circular surface flaw on a parallel plane is evaluated as a function of the vertical and horizontal separation distance as well as the relative crack sizes of the two cracks. It is found that all three parameters affect the magnitude of the maximum SIFs and the SIF distribution behavior along the crack front. It is also found the maximum SIFs along the crack front varying with the horizontal spacing S/a_2 behave differently compared with their 2-D counterparts. The present 3-D results show that the existing alignment rules used to evaluate the "fitness for service" do not agree and can lead to distinctly opposite results, which can prove to be disastrous. Also, the results presented in this paper use a circular representation for the embedded crack and a quarter circle for the edge crack which have been shown not to be the most dangerous representations of 3-D cracks [e.g., 19]; i.e., there are elliptic crack configurations that are more dangerous. Thus, more work need to be done to bring these codes under one acceptable set of rules.

Acknowledgements

This work used the Extreme Science and Engineering Discovery Environment (XSEDE), which is supported by National Science Foundation grant number PSC Grant MSS140004P. The first author (QM) acknowledges the support from his University through the Faculty Development Grant.

References

[1] Y. Okamura, A, Sakashita, T. Fukuda, H. Yamashita, T. Futami, Latest SCC Issues of Core Shroud and recirculation Piping in Japanese BWRs, Trans. Of 17th Int. Conf. on Structural Mechanics in Reactor Technology (SMiRT 17), Prague, WG01-1, 2003.
[2] M. Kamaya, T. Haruna, Crack Initiation Model for Type 304 Stainless Steel in High Temperature Water, Corrosion Science, 48 (2006) 2442-56.
[3] ASME, B&PV Code Section XI, 2007.
[4] British Standards, BritS 7910, 2005.
[5] European Fitness-for-Service Network (FITNET), GTC1- 2001-43049.
[6] American Petroleum Institute, Fitness-for-Service, API 579-1/ASME FFS-1, 2007.
[7] The Japan Society of Mechanical Engineers, Rules on Fitness-for-Service for Nuclear Power Plant, JSME S NA1-2008 (in Japanese), 2008.
[8] M. Kamaya, Growth evaluation of multiple interacting surface cracks. Part I: Experiments and simulation of coalesced crack, Engineering Fracture Mechanics 75 (2008) 1350–1366.
[9] K. Hasegawa, K. Saito, K. Miyazaki, Alignment Rule for Non-Aligned Flaws for Fitness-for-Service Evaluations Based on LEFM, ASME JPVT, 131 (2009) 041403-1.
[10] K. Hasegawa, K. Miyazai, K. Saito, Behavior of plastic collapse moments for pipes with two non-aligned flaws, ASME PVP2010-25199, Bellevue, Washington, July 18-22, 2010.
[11] K. Hasegawa, K. Miyazaki, K. Saito, Plastic collapse loads for flat plates with dissimilar Non-aligned through-wall cracks, ASME PVP2011-57841, July 17-21, Baltimore, Maryland, USA, 2011.
[12] K. Miyazaki, K. Hasegawa, K. Saito, Effect of flaw dimensions on ductile fracture behavior of non-aligned multiple flaws in a plate, ASME PVP2011-57559, July 17-21, Baltimore, Maryland, USA, 2011.
[13] K. Suga, K. Miyazaki, S. Kawasaki, Y. Arai, Study on the interaction of multiple flaws in ductile fracture process, ASME PVP2011-57188, July 17-21, Baltimore, Maryland, USA, 2011.
[14] K. Suga, K. Miyazaki, R. Senda, M. Kikuchi, Ductile fracture simulation of multiple surface flaws, ASME PVP2011-57147, July 17-21, Baltimore, Maryland, USA, 2011.
[15] Q. Ma, C. Levy, M. Perl, A LEFM Based Study on the Interaction between an Edge and an Embedded Parallel Crack, ASME PVP2013, July 14-18, Paris, France, 2013.
[16] Swanson Analysis System Inc., ANSYS 12 User Manual, 2009.
[17] Q, Ma, Stress Concentration and Stress Intensity Factors of a Multi-eroded, Cracked Autofrettaged Pressurized Thick-Walled Cylinder, Master's thesis, FIU, 1999.
[18] C. Levy, M. Perl, Q. Ma, The Influence of Multiple Axial Erosions on a Three-Dimensional Crack in Determining the Fatigue Life of Autofrettaged Pressurized Cylinders, ASME JPVT, 124(1) 1-6. doi: 10.1115/1.1386656, 2001.
[19] C. Levy, M. Perl, N. Kokkavessis, Three-Dimensional Interaction Effects in an Internally Multicracked Pressurized Thick-Walled Cylinder. Part II - Longitudinal Coplanar Crack Arrays, ASME JPVT, 118 (1996) 364-368.